Annals of Anatomy 216 (2018) 112–119

Contents lists available at ScienceDirect

Annals of Anatomy

journal homepage: www.elsevier.com/locate/aanat

Early molecular response and microanatomical changes in the masseter muscle and mandibular head after botulinum toxin intervention in adult mice☆

Julián Balanta-Melo[a,b], Viviana Toro-Ibacache[a,c,d], Maria Angélica Torres-Quintana[e], Kornelius Kupczik[f], Carolina Vega[a], Camilo Morales[a,g,h], Nadia Hernández-Moya[a], Manuel Arias-Calderón[a,h], Carolina Beato[a,h], Sonja Buvinic[a,*]

[a] Institute for Research in Dental Sciences, Faculty of Dentistry, Universidad de Chile, Chile
[b] School of Dentistry, Universidad del Valle, Colombia
[c] Quantitative Analysis Center in Dental Anthropology, Faculty of Dentistry, Universidad de Chile, Chile
[d] Department of Human Evolution, Max Planck Institute for Evolutionary Anthropology, Germany
[e] Department of Pathology and Oral Medicine, Faculty of Dentistry, Universidad de Chile, Chile
[f] Max Planck Weizmann Center for Integrative Archaeology and Anthropology, Max Planck Institute for Evolutionary Anthropology, Germany
[g] Department of Basic Sciences, Health Faculty, Pontificia Universidad Javeriana, Colombia
[h] Institute of Biomedical Sciences, Faculty of Medicine, Universidad de Chile, Chile

ARTICLE INFO

Article history:
Received 24 August 2017
Received in revised form
22 November 2017
Accepted 27 November 2017

Keywords:
Masseter muscle atrophy
Botulinum toxin type A
Mandibular head
Bone loss

ABSTRACT

Background: Masseter muscle paralysis induced by botulinum toxin type A (BoNTA) evokes subchondral bone loss in mandibular heads of adult rats and growing mice after 4 weeks. However, the primary cellular and molecular events leading to altered bone remodeling remain unexplored. Thus, the aim of the current work has been to assess the molecular response that precedes the early microanatomical changes in the masseter muscle and subchondral bone of the mandibular head in adult mice after BoNTA intervention.
Methods: A pre-clinical *in vivo* study was performed by a single intramuscular injection of 0.2 U BoNTA in the right masseter (experimental) of adult BALB/c mice. The contralateral masseter was injected with vehicle (control). Changes in mRNA levels of molecular markers of bone loss or muscle atrophy/regeneration were addressed by qPCR at day 2 or 7, respectively. mRNA levels of receptor activator of nuclear factor-κB ligand (RANKL) was assessed in mandibular heads, whilst mRNA levels of Atrogin-1/MAFbx, MuRF-1 and Myogenin were addressed in masseter muscles. In order to identify the early microanatomical changes at day 14, fiber diameters in transversal sections of masseter muscles were quantified, and histomorphometric analysis was used to determine the bone per tissue area and the trabecular thickness of subchondral bone of the mandibular heads.
Results: An increase of up to 4-fold in RANKL mRNA levels were detected in mandibular heads of the BoNTA-injected sides as early as 2 days after intervention. Moreover, a 4–6 fold increase in Atrogin-1/MAFbx and MuRF-1 and an up to 25 fold increase in Myogenin mRNA level were detected in masseter muscles 7 days after BoNTA injections. Masseter muscle mass, as well as individual muscle fiber diameter, were significantly reduced in BoNTA-injected side after 14 days post-intervention. At the same time, in the mandibular heads from the treated side, the subchondral bone loss was evinced by a significant reduction in bone per tissue area (−40%) and trabecular thickness (−55%).
Conclusions: Our results show that masseter muscle paralysis induced by BoNTA leads to significant microanatomical changes by day 14, preceded by molecular changes as early as 2 days in bone, and 7 days in muscle. Therefore, masseter muscle atrophy and subchondral bone loss detected at 14 days are preceded by molecular responses that occur during the first week after BoNTA intervention.

Abbreviations: BoNTA, botulinum toxin type A; RANKL, receptor activator of nuclear factor-κB ligand; Atrogin-1/MAFbx, Atrogin-1/Muscle atrophy F-box; MuRF-1, muscle RING finger 1; Myo, myogenin; Cav3, caveolin-3; B.Ar/T.Ar, bone per tissue area; Tb.Th, trabecular thickness.

☆ This paper belongs to the special issue Dentomaxillary.

* Corresponding author at: Institute for Research in Dental Sciences, Faculty of Dentistry, Universidad de Chile, Sergio Livingstone Pohlhammer 943, 8380492 Santiago, Chile.
E-mail address: sbuvinic@u.uchile.cl (S. Buvinic).

https://doi.org/10.1016/j.aanat.2017.11.009
0940-9602/

1. Introduction

The temporomandibular joint (TMJ) is found exclusively in mammals, and is a specialized structure that articulates the mandibular head in the condylar process of the mandible with the mandibular fossa of the squamous part of the temporal bone (Herring, 2003; Suzuki and Iwata, 2016). Bone components of the TMJ respond to mechanical stimuli from masticatory muscles (Toro-Ibacache and O'Higgins, 2016); the synchronous contraction of these muscles produces the mandibular movements that are required for vital functions such as mastication and defense (Baverstock et al., 2013; Cox et al., 2012). In order to perform these activities, the mammalian masticatory apparatus has evolved from the interaction of different tissues like skeletal muscle, bones, and teeth (Cox et al., 2012; Tiphaine et al., 2013). Also, the adaptation of the masticatory apparatus during development, and to different environmental conditions such as changes in hardness of diet and/or masticatory loadings (Spassov et al., 2017) has been successfully achieved because of masticatory muscle plasticity (Abe et al., 2007) and the craniofacial changes through the bone remodeling process (Anderson et al., 2014).

Bone tissue homeostasis depends on the physiological process, named bone remodeling, involving resorption of damaged bone, and subsequent replacement by newly formed mineralized tissue (Sims and Martin, 2014). Local bone loss, due to increased bone resorption over bone apposition, is evoked by skeletal muscle paralysis induced by the intramuscular injection of botulinum toxin type A (BoNTA) (Aliprantis et al., 2012; Recidoro et al., 2014). This neurotoxin is a potent blocker of acetylcholine release at the neuromuscular junction, leading to temporal muscle paralysis, loss of muscle mass, and progressive muscle atrophy (Pirazzini et al., 2017; Rossetto et al., 2014). Since the consequences of the intramuscular injection of this neurotoxin are not limited to the targeted muscles, there are many aspects of the interactions between skeletal muscle and bone that remain unexplored. This is particularly the case for the masticatory apparatus. In this context, masseter muscle paralysis induced by BoNTA in adult rats (Kun-Darbois et al., 2015) and growing mice (Dutra et al., 2016) produces subchondral bone loss at the mandibular head after 4 weeks of intervention. However, tissue changes and the cellular and molecular responses preceding this effect are not completely understood. When assessed in hind limb muscles of adult mice, BoNTA-induced muscle paralysis increases the expression of muscle atrophy markers (Vegger et al., 2016) and of a bone resorption promoter (receptor activator of nuclear factor κ-B ligand, RANKL), as early as 7 days after intervention (Aliprantis et al., 2012; Marchand-Libouban et al., 2013). Moreover, there is an increase in the use of BoNTA in humans as a therapeutic approach in temporomandibular disorders, aesthetic complains, and parafunctions, with the masseter muscle as direct target (Chen et al., 2015; Fedorowicz et al., 2013; Miller and Clarkson, 2016; Soares et al., 2014; Tinastepe et al., 2015). However, BoNTA has not been approved (i.e. by the Food and Drug Administration) for use in the masseter muscle, and there is a lack of preclinical evidence regarding the safety of this intervention in the masticatory apparatus (Pirazzini et al., 2017).

There are still unanswered questions about the morphological and molecular events relating to masticatory muscle paralysis, which are relevant from an anatomical, physiological, and, ultimately, clinical perspective. In the present work, we developed a mouse model of a unilateral masseter muscle paralysis induced by BoNTA injections to unveil the microanatomical changes in treated masseter muscles and subjacent mandibular heads after 14 days post-intervention. We hypothesized that a molecular response involving changes in expression of muscle atrophy and bone resorption markers precedes detectable masseter muscle atrophy, as well as subchondral bone loss in mandibular heads after a single BoNTA injection.

2. Materials and methods

2.1. Animals

Sixteen adult male BALB/c mice (8 weeks old) between 18 g–25 g were obtained from the Experimental Platform of the Faculty of Dentistry (Universidad de Chile). Standard animal room conditions (48–50% humidity; 20 ± 2 °C; 12 h light/dark cycle), and water and food (LabDiet® JL Rat and Mouse/Auto 6F 5K67) *ad libitum* were used. Mice were divided in one control group (n = 5) and three experimental groups: BoNTA 2d (n = 3), BoNTA 7d (n = 3), and BoNTA 14d (n = 5) after BoNTA injection. The number of animals for each time period was selected to ensure a minimum of n = 3 for each experimental technique. All *in vivo* protocols were approved by the Bioethics Committee for Animal Research of the Faculty of Dentistry of Universidad de Chile (N° FOUCH061501).

2.2. Intervention

A control group of mice bilaterally injected with saline solution in the masseter muscles was maintained for 14 days before euthanasia, as a reference to compare the welfare state of mice unilaterally injected with BoNTA. Each of the mice of the experimental groups received one single intramuscular injection of botulinum toxin type A (0.2 U; 10 μl; *Onabotulinumtoxin A*; BOTOX®, Allergan Chile; Lot #. C3837 C3) in the right masseter muscle (BoNTA). Dosage and volume were based in previous reports (Aliprantis et al., 2012; Dutra et al., 2016; Lodberg et al., 2015), also considering LD50 (Rossetto et al., 2014) and mean body weight. The left masseter muscle was injected with the same volume of saline solution (NaCl, 0.9% p/v), and served as intra-individual control. Injections were performed by a veterinarian, without previous anesthesia, maintaining an angle and depth previously validated as safe. Body mass was quantified daily from day 0 (before intervention) to the end of experiment for each group. Incisor lengths as well as animal welfare parameters were examined daily. After 2 days, 7 days, or 14 days of intervention (for experimental groups) or 14 days (for control group), animals were euthanized by cervical dislocation. Then, masseter muscles were promptly dissected and weighed. After this procedure, mouse mandibles were separated at the middle cartilaginous junction, and manually dislocated for a complete removal. This procedure provided one hemi-mandible from the right or experimental side (BoNTA), and one from the left side (control) per animal.

2.3. Total RNA extraction and reverse transcription

To assess mRNA expression, mandibular heads from mice of group 2d (n = 3) were carefully cut off from the mandibular ramus with hard tissue scissors. These samples were mechanically disrupted in 1 ml of Trizol™ (Life Technologies, CA, USA), and stored at −80 °C until processing. The same procedure was performed with the masseter muscles from mice of group 7d (n = 3). According to the Trizol™ manufacturer's instructions, total RNA was obtained. RNA was diluted in 20 μl (bone) or 40 μl (muscle) of nuclease-free water and quantified by spectrophotometry (absorbance at 260 nm).

The cDNA from bone was obtained from 2 μg RNA by using the High-Capacity cDNA Reverse Transcription Kit (Life Technologies, CA, USA) in a 20 μl final volume. In addition, cDNA from masseter muscles was obtained from 1 μg RNA by using ImProm-II™ Reverse Transcription System (Promega, WI, USA), in a final reaction volume of 20 μl. Subsequently, DNA-free™ DNA Removal Kit was

used (Life Technologies, CA, USA). To exclude any contamination with genomic DNA, negative controls were performed by replacing Reverse Transcriptase with nuclease-free water.

2.4. Quantitative real-time PCR (qRT-PCR)

Rankl, Atrogin-1/MAFbx, MuRF-1, and *Myogenin* mRNA expression was assessed by using qRT-PCR. *Gapdh* and *18S* served as housekeepings in muscle and bone-derived samples, respectively. The primers used were as follows: *Rankl forward:* 5′-TGGAAGGCTCATGGTTGGAT-3′, *reverse:* 5′-CATTGATGGTGAGGTGTGCAA (Swanson et al., 2006); *Atrogin-1/MAFbx forward:* 5′-GTTTTCAGCAGGCCAAGAAG-3′, *reverse:* 5′-TTGCCAGAGAACACGCTATG-3′ (Murphy et al., 2012); *MuRF-1 forward:* 5′-TGCCTACTTGCTCCTTGT-3′, *reverse:* 5′-CTGGTGGCTATTCTCCTT-3′ (Murphy et al., 2012); *Myogenin forward:* 5′-CTCCCTTACGTCCATCGT-3′, *reverse:* 5′-CAGGACAGCCCCACTTAA-3′ (Church et al., 2014); *18S forward:* 5′-GGGCCCGAAGCGTTTACTTT-3′, *reverse:* 5′-TTGCGCCGGTCCAAGAATTT-3′ (Valladares et al., 2013); *Gapdh forward:* 5′-CAACTTTGGCATTGTGGAAG-3′, *reverse:* 5′-CTGCTTCACCACCTTCTTG-3′ (Bustamante et al., 2014). All primers used presented optimal amplification efficiency (between 90 and 110%). qPCR was performed using Fast SYBR® Green Master Mix and the StepOne™ Real-Time PCR System from Thermo Fischer Scientific (Waltham, MA, USA). Thermocycling conditions were as follows: 95 °C for 20 s previous to 40 cycles of 95 °C for 3 s and 60 °C for 30 s. CT value was determined by StepOne software when fluorescence was 25% higher than background. PCR products were verified by melting curve analysis. Expression values were normalized to housekeeping and are reported in units of $2^{-\Delta\Delta CT} \pm$ standard error of the mean (SEM) as described (Pfaffl, 2001).

2.5. Immunofluorescence

Right and left masseter muscles from one mouse (Group 14d; n = 1 per side) were dissected, immediately frozen for 1 min by performing an isopentane/liquid nitrogen protocol (Meng et al., 2014) and stored at −80 °C until processing.

Frozen sections of 4 μm thickness from the middle of each masseter muscle were obtained and placed on StarFrost® slides (Knittel Glaser, Germany). Then, these sections were rinsed three times with PBS, fixed with 4% PFA for 30 min at room temperature, and pre-incubated twice with 100 mM glycine in PBS for 5 min. Membrane permeabilization was performed with 0.1% Tritón X100 for 10 min at room temperature, and then all samples were pre-incubated with 4% BSA at room temperature for blocking unspecific binding of primary antibody. Mouse monoclonal caveolin3 (Cav3) antibody (BD Bioscience, CA, USA) was used to detect individual muscle fiber's outer perimeter. Primary antibody was incubated overnight at 4 °C. Detection of Cav3 was carried out with an Alexa-488 conjugated antibody (Life Technologies, CA, USA) incubated for 30 min at 37 °C in dark environment. DAPI was used for nuclear staining, and DACO was the mounting medium. Digital images were obtained by using an Eclipse Ti-E Inverted Fluorescence Microscope (Nikon®) with 40× objectives. Feret's diameter of individual masseter muscle fibers was quantified with the ImageJ 1.51h software (Schneider et al., 2012).

2.6. Bone histomorphometry

After dissection, each hemi-mandible from the mice of group 14d (n = 3 per side) was placed in formalin solution (neutral buffered, 10%) for 24 h at 4 °C with agitation (Mack et al., 2014; Marino et al., 2016). Samples were rinsed three times for 1 h with PBS and then decalcified by using neutral 12% EDTA for 14 days at 4 °C with agitation (manual puncture and X-ray images were used to verify decalcification). Hemi-mandibles were rinsed three times-1 h each with 100 mM $MgCl_2$ and stored in distilled water for 24 h. Sections of the longitudinal axis of the mandibular head were obtained. Samples were embedded in paraffin blocks and coronal sections of 4 μm from the middle volume of each mandibular head were obtained and placed in individual slides. Then, Goldner's trichrome staining was performed in single representative slices from right and left mandibular heads, derived from the same anatomical level. Image acquisition was performed with a Binocular Microscope Axio Lab.A1 (with phototube, 10× and 40× objectives) coupled to a Reflex Canon T3 camera. Bone per tissue area (B.Ar/T.Ar) and Trabecular Thickness (Tb.Th) of subchondral bone were quantified by using OsteoidHisto, an open source software for semi-automated bone histomorphometry (van 't Hof et al., 2017).

2.7. Statistical analysis

As a preliminary study, a small sample size was considered (n = 3–5) (Thabane et al., 2010). Results are reported as Mean ± SEM. Differences between BoNTA and Control sides were determined with the Mann–Whitney test and the Wilcoxon signed-rank test (*p*-value was set at 0.05) by using GraphPad Prism version 7.0b for Mac OS X (GraphPad Software, CA, USA).

3. Results

3.1. General findings on the animal model

Throughout the study, mice from control and BoNTA groups showed a similar increase in body mass. The length of the incisors, their external appearance and behavior were daily controlled and registered. There was no teeth overgrowth or detectable discomfort or stress in any group (control and BoNTA). Also, in all the experimental groups (BoNTA 2d, 7d and 14d), a qualitative flattened aspect of the injected masseter was observed after 30 min of intervention, compared with the control side injected with saline solution.

3.2. BoNTA-induced masseter paralysis promotes an early molecular response in muscle and bone

As soon as 2 days after BoNTA intervention, a 4-fold increase in the mRNA levels of the bone resorption promoter RANKL was detected in the mandibular heads derived from the experimental side (Fig. 1A). On the other hand, a 4–6 fold increase in mRNA levels for atrophy markers (Atrogin-1/MAFbx and MuRF-1) and a 25 fold increase in a muscle regeneration marker (Myogenin) was observed in BoNTA-injected masseter muscles (Fig. 1B).

3.3. Microanatomical changes of masseter muscle after BoNTA injection

A reduction in masseter muscle mass was detectable in the BoNTA-injected side of all experimental groups, but it was only significant after 14 days (−18%), when compared with the control sides (Fig. 2A). Moreover, a reduction in the masseter volume can be observed after 14 days of BoNTA intervention (Fig. 2B). Masseter muscle atrophy was evidenced by Cav3 staining as a reduction in individual muscle fiber cross-sectional area in BoNTA injected muscles (Fig. 3A), compared with the contralateral control side (Fig. 3B). There was no evidence of fibrosis or muscle central nuclei (indicator of muscle repair) in both control and experimental muscles.

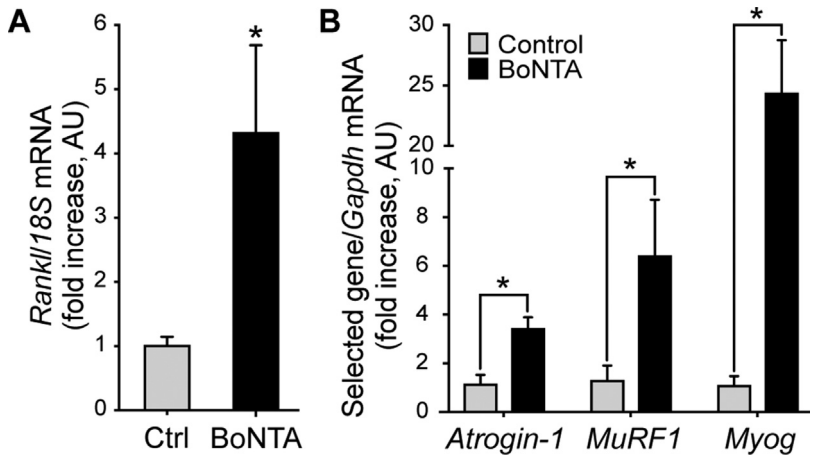

Fig. 1. BoNTA intervention in masseter muscle increases the gene expression of muscular atrophy/regeneration and bone-resorption markers. Tissues (masseter muscle and mandibular head) were dissected and isolated at the indicated time. Total RNA was obtained and retrotranscribed. mRNA of selected genes was addressed by qPCR. (A) In mandibular head samples, mRNA of *Rankl* showed a 4.2-fold increase in the experimental side versus control 2 days after injection (n = 3; Mean ± SEM; **p-value* < 0.05; Mann–Whitney test). (B) In masseter muscle samples, mRNA relative expression of *Atrogin-1/MAFbx*, *MuRF-1*, and *Myogenin (Myog)* was significantly increased in experimental side compared with control at 7 days (n = 3).

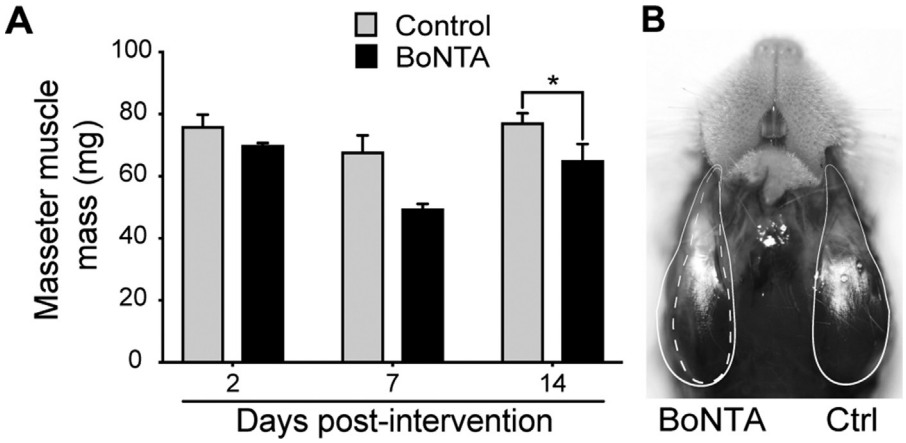

Fig. 2. BoNTA injection significantly reduces masseter muscle mass after 14 days. A single BoNTA injection (0.2 U/10 μl) was performed in the right masseter muscle. Left masseter muscle was injected with vehicle (saline solution) as an intra-individual control. (A) Masseter muscle mass from all experimental groups assessed at different days post-intervention; n = 3–5; Mean ± SEM; *: $p < 0.05$; Wilcoxon signed-rank test. (B) Ventral view of masseter muscle *in situ* at 14 days post-intervention. Dashed white line shows right masseter muscle perimeter compared with left masseter muscle perimeter (solid white line). A representative photo is shown.

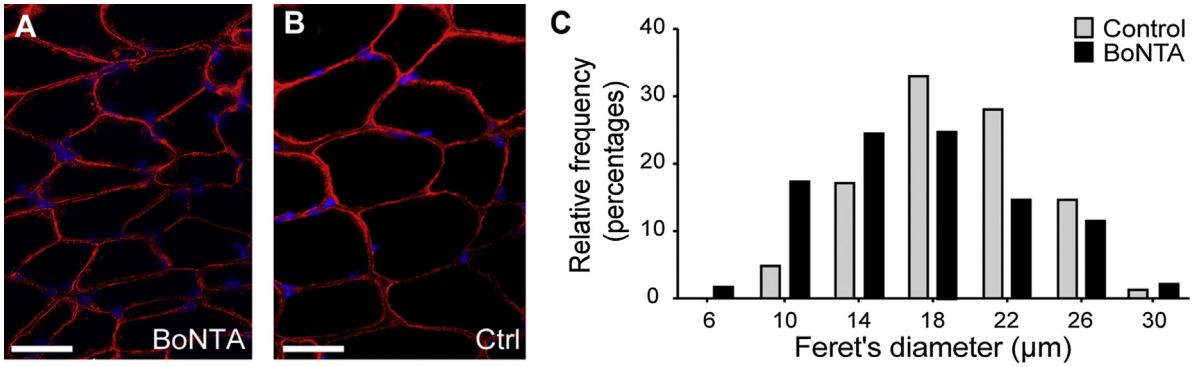

Fig. 3. BoNTA injection reduces the diameter of masseter muscle fibers. Masseter muscles dissected 14 days after BoNTA (A) or saline solution (B) injection were cryosectioned. Immunofluorescence was performed against Cav3 (red) to delimit cellular perimeter. Nucleus were stained with DAPI (blue). Digital images were obtained by using a Ti-E Inverted Fluorescence Microscope (Nikon®) with 40× objectives. C. Feret's diameter of individual masseter muscle fibers was quantified from fluorescence images by using the ImageJ 1.51h software. The histogram shows the frequency of diameters for 224 individual masseter muscle fibers per side, and confirms the higher frequency of smaller diameters in the experimental side. Scale bar: 20 μm. (For interpretation of the references to color in this figure legend, the reader is referred to the web version of this article.)

In addition, the quantification of individual fibers Feretís diameter showed an increase in the relative frequency of smaller fibers in BoNTA injected muscles, as compared with contralateral control (Fig. 3C).

3.4. Microanatomical changes in subjacent mandibular heads after BoNTA-induced masseter muscle paralysis

The histological slices of the mandibular heads (BoNTA 14d group; cutting plane in Fig. 4A) showed a qualitative increase in the medullary spaces of the trabecular bone in the BoNTA-injected side, compared with the control side (Fig. 4B and C). Digital quantification of subchondral bone parameters by histomorphometric analysis showed that both the B.Ar/T.Ar and the Tb.Th were significantly reduced in the BoNTA-injected side (Fig. 4D–E).

4. Discussion

In this study, we demonstrate that BoNTA-induced masseter muscle paralysis in adult mice produces masseter muscle atrophy and bone loss in the subjacent mandibular head. In addition, these microanatomical changes are preceded by early increments in the mRNA levels of RANKL in the bone and Atrogin-1/MAFbx, MuRF-1 and Myogenin in muscles during the first week after BoNTA intervention. These findings support the hypothesis that a specific molecular response precedes the detectable subchondral bone loss in mandibular head, and define the masseter muscle atrophy after a single BoNTA intervention. Also, this study evinces subchondral bone loss in the mandibular head only 14 days after BoNTA injection, earlier than previous studies that report this finding in rodents after 4 weeks (Dutra et al., 2016; Kun-Darbois et al., 2015).

In mice, *Atrogin-1/MAFbx, MuRF-1*, and *Myogenin* expression is required for skeletal muscle degradation during denervation-induced atrophy (Baumann et al., 2016; Macpherson et al., 2011). Similar to denervation, the mechanism of action of BoNTA blocks the neuromuscular transmission, and leads to reversible muscle paralysis (Pirazzini et al., 2017; Rossetto et al., 2014). *Rectus femoris* muscles from female C57BL/6 mice injected with BoNTA showed a significant increase in gene expression for *Atrogin-1/MAFbx* and *MuRF-1* after 7 days and 14 days post-intervention, but not at day 21, compared with control hindlimbs (Vegger et al., 2016). Interestingly, our results also show that BoNTA-injected masseter muscles increased the expression of *Atrogin-1/MAFbx, MuRF-1*, and *Myogenin* after 7 days, suggesting a conserved mechanism in a different mouse strain, and a different muscle type. The latter is relevant, considering that craniofacial muscles are different from those of the trunk and limbs (Sciote et al., 2003). Despite defined anatomical limits such as the segmented pattern of trunk (somites), craniofacial muscles are characterized by specific and particular gene expression zones (or molecular limits) during embryonic development from cranial mesoderm (Michailovici et al., 2015; Sambasivan et al., 2011). Also, adult masticatory muscles such as masseter express embryonic and α-cardiac myosin heavy chains, which are absent in mature trunk and limb muscles (Schiaffino and Reggiani, 2011). In addition, craniofacial muscles are capable of performing fine actions such as facial expression and mandibular movements (Michailovici et al., 2015; Sambasivan et al., 2011; Sciote et al., 2003). Previous studies using BoNTA injection in masseter muscle of rodents have only described a muscle volume reduction either by measuring its width (Moon et al., 2015), by visual inspection (Kun-Darbois et al., 2015), or without any further evaluation (Dutra et al., 2016). In the current study, we performed quantitative measurements related to masseter muscle mass and individual muscle fiber diameter, by implementing an adapted protocol with a reproducible technique (Bonetto et al., 2015; Briguet et al., 2004). Thus, we determined that BoNTA intervention promoted significant loss of muscle mass and size after 14 days. Taken together, the observed molecular and microstructural changes validate our protocol as a proper mechanism to evoke masseter atrophy in adult mice.

RANKL is required for osteoclastogenesis and bone resorption promotion (Takahashi et al., 1999). BoNTA intervention in quadriceps and calf muscles leads to a bone loss between 43.2%–53.4% in subjacent femur and tibia of female C57BL/6 mice after 21 days (Warner et al., 2006). Bone marrow gene expression of *Rankl* from femurs (Marchand-Libouban et al., 2013) of proximal tibia metaphysis (Aliprantis et al., 2012) is significantly increased after 7 days of BoNTA intervention in the same model. However, another study with female C57BL/6 mice reports no significant differences in *Rankl* expression between distal tibia from experimental side compared with control from day 7 to day 21 post-intervention (Vegger et al., 2016). Also, the time for these outcomes may differ according to the explored zone (i.e. metaphysis versus diaphysis) (Ausk et al., 2013). However, these studies evaluate the degradation of long bones in lower limbs, and osteoclasts from craniofacial bones (which also have a different embryological origin) may degrade mineralized tissue by different mechanisms and degrees (Everts et al., 2006; Santagati and Rijli, 2003). In addition, C57BL/6 mice are more liable to bone loss after BoNTA intervention in lower limbs than BALB/c mice (Lodberg et al., 2015), which may impair the comparisons between strains. Our study demonstrates a significant increase in *Rankl* expression in complete mandibular heads as early as 2 days after BoNTA intervention, leading to the question of the specific cells involved in this early response. After 14 days, our findings show a bone loss of 30% (B.Ar/T.Ar) in mandibular heads from experimental versus control side; this effect is consistent with those found in adult male rats (−35%) (Kun-Darbois et al., 2015), and larger than the — 21.4% reported in female CD-1 growing mice (Dutra et al., 2016) after 4 weeks. This difference between male and female animals may suggest a sex contribution to the intervention's outcome.

Considering the lack of published data on the topic, sample size calculation was not possible, so performing a preliminary work with n = 3–5 animals per condition. The main scope was to test feasibility and safety to obtain a mice model of BoNTA-evoked masseter paralysis, and address histologic and gene expression changes in mandible head. Statistical differences obtained in Control- and BoNTA- masseter muscle (weight, volume, fibers diameter and gene expression), as well as in mandible head (gene expression and histomorphometric parameters), provide a basis for the proper selection of sample size in future extended studies.

Our adult mouse model of unilateral masseter muscle paralysis induced by BoNTA will allow for studies of the cellular and molecular mechanisms that promote the subchondral bone loss in the mandibular head after a single intervention. Although our results are strictly limited to adult male BALB/c mice, some of these effects of BoNTA have been found in adult rats and growing mice. Female mice should also be studied in order to assess the effect of other factors such as hormonal status or the degree of muscle development. Also, it should be pointed out that different strains may exhibit different degrees of bone loss after BoNTA-induced muscle paralysis, as suggested by a comparative study (Lodberg et al., 2015). However, it is important to note that subchondral bone loss after BoNTA injection in masseter muscle has been also evinced in other mammals such as rabbits, but only after 4 weeks and 12 weeks post-intervention (Rafferty et al., 2012). Thus, structural changes of the mandibular head could be a potential adverse effect maintained across mammalian species including humans, as suggested by a pilot study that found detectable bone loss in mandibular heads of women treated with BoNTA injections in masseter muscles for oral pain (Raphael et al., 2014). Therefore, since BoNTA intervention is a current common practice in dentistry for several health-related

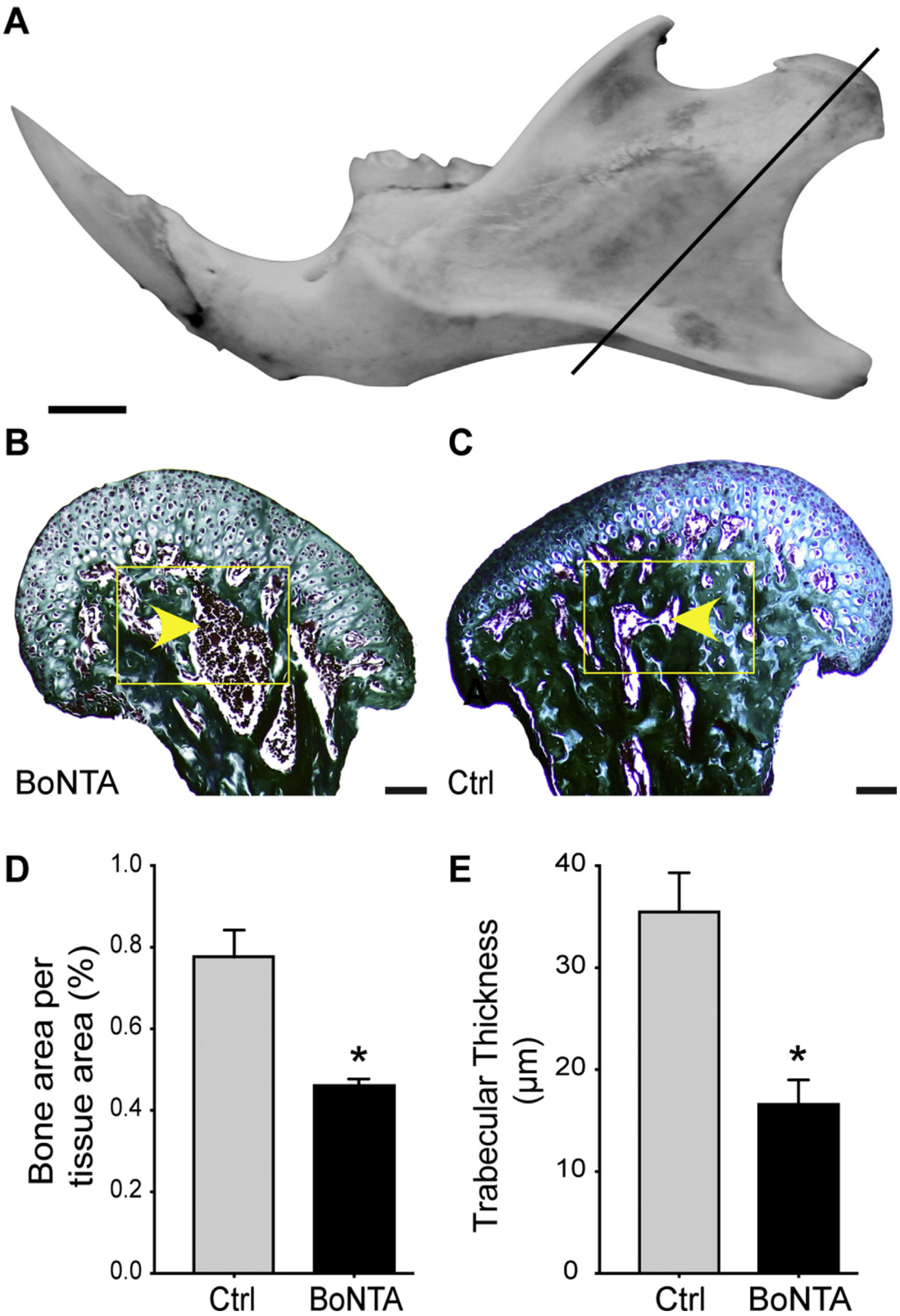

Fig. 4. BoNTA-induced masseter muscle paralysis promotes bone loss in the subjacent mandibular head. 14 days after BoNTA or saline solution injection in masseter muscles, hemi-mandibles were isolated and processed for histomorphometry. Digital images of Goldner's trichrome stain were performed with a Binocular Microscope Axio Lab.A1. (A) Cutting plane of the histological section relative to the anatomy of the mouse mandible (1:1 macro-photograph of real dissected left mandible from vestibular side). Scale bar: 1 mm. Representative 10× image of mandibular head from BoNTA-injected side (B) reveals an increase in medullary spaces of trabecular bone (yellow arrow heads) compared with control side (C). Histomorphometric parameters of bone area per tissue area (D) and trabecular thickness (E) confirm a significant subchondral bone loss after 14 days of intervention. Region of interest = yellow rectangle. Scale bar: 100 µm (n = 3; Mean ± SEM; *p-value <0.05; Mann–Whitney test). (For interpretation of the references to color in this figure legend, the reader is referred to the web version of this article.)

issues such as temporomandibular disorders, but also in aesthetics, our research may contribute with preclinical results to determine the risk of adverse reactions of such interventions in masticatory muscles and neighboring tissues. In addition, our approach will advance the understanding of the cellular and molecular mechanisms behind the adaptive response of the masticatory apparatus of mammals to different stimuli.

5. Conclusions

Masseter muscle paralysis induced by BoNTA leads to masseter muscle atrophy and to the subchondral bone loss of the associated mandibular head, detected after 2 weeks. These morphological findings are preceded by early changes in tissue specific gene expression that should be assessed during the first week after BoNTA intervention. RANKL mRNA levels increased in mandible heads as early as 2 days after BoNTA intervention, while muscle atrophy and regeneration markers rise after 7 days in the treated masseter muscles. Thus, we are currently developing an extended study to address the possibility that bone microanatomical changes appear even before 14 days, or be even greater after this period of time.

Funding

This work was supported by the FONDECYT Chile Grants No. 1151353 (SB) and No. 11150175 (VT-I); CONICYT Chile Scholarship No. 21170015 (JB), No. 63140009 (CM), No. 21150059 (CB), No. 21151035 (MAC); and the Program Professor Scholarship Semillero Docente 2014 of the Universidad del Valle, Colombia (JB).

Acknowledgment

We thank Cristian Campos from Institute of Biomedical Sciences (Faculty of Medicine, Universidad de Chile. Santiago, Chile) for assistance with the masseter muscle freezing technique, and the cryosectioning process for immunofluorescence analyses.

References

Abe, S., Sakiyama, K., Ide, Y., 2007. Muscle plasticity: changes in oral function of muscle fiber characteristics. J. Oral Biosci. 49, 219–223.
Aliprantis, A.O., Stolina, M., Kostenuik, P.J., Poliachik, S.L., Warner, S.E., Bain, S.D., Gross, T.S., 2012. Transient muscle paralysis degrades bone via rapid osteoclastogenesis. FASEB J. 26, 1110–1118.
Anderson, P.S., Renaud, S., Rayfield, E.J., 2014. Adaptive plasticity in the mouse mandible. BMC Evol. Biol. 14, 85.
Ausk, B.J., Huber, P., Srinivasan, S., Bain, S.D., Kwon, R.Y., McNamara, E.A., Poliachik, S.L., Sybrowsky, C.L., Gross, T.S., 2013. Metaphyseal and diaphyseal bone loss in the tibia following transient muscle paralysis are spatiotemporally distinct resorption events. Bone 57, 413–422.
Baumann, C.W., Liu, H.M., Thompson, L.V., 2016. Denervation-induced activation of the ubiquitin-proteasome system reduces skeletal muscle quantity not quality. PLoS One 11, e0160839.
Baverstock, H., Jeffery, N.S., Cobb, S.N., 2013. The morphology of the mouse masticatory musculature. J. Anat. 223, 46–60.
Bonetto, A., Andersson, D.C., Waning, D.L., 2015. Assessment of muscle mass and strength in mice. Bonekey Rep. 4, 732.
Briguet, A., Courdier-Fruh, I., Foster, M., Meier, T., Magyar, J.P., 2004. Histological parameters for the quantitative assessment of muscular dystrophy in the mdx-mouse. Neuromuscul. Disord. 14, 675–682.
Bustamante, M., Fernandez-Verdejo, R., Jaimovich, E., Buvinic, S., 2014. Electrical stimulation induces IL-6 in skeletal muscle through extracellular ATP by activating Ca(2+) signals and an IL-6 autocrine loop. Am. J. Physiol. Endocrinol. Metab. 306, E869–E882.
Chen, Y.W., Chiu, Y.W., Chen, C.Y., Chuang, S.K., 2015. Botulinum toxin therapy for temporomandibular joint disorders: a systematic review of randomized controlled trials. Int. J. Oral. Maxillofac. Surg. 44, 1018–1026.
Church, J.E., Trieu, J., Sheorey, R., Chee, A.Y., Naim, T., Baum, D.M., Ryall, J.G., Gregorevic, P., Lynch, G.S., 2014. Functional beta-adrenoceptors are important for early muscle regeneration in mice through effects on myoblast proliferation and differentiation. PLoS One 9, e101379.
Cox, P.G., Rayfield, E.J., Fagan, M.J., Herrel, A., Pataky, T.C., Jeffery, N., 2012. Functional evolution of the feeding system in rodents. PLoS One 7, e36299.
Dutra, E.H., O'Brien, M.H., Lima, A., Kalajzic, Z., Tadinada, A., Nanda, R., Yadav, S., 2016. Cellular and matrix response of the mandibular condylar cartilage to botulinum toxin. PLoS One 11, e0164599.
Everts, V., Korper, W., Hoeben, K.A., Jansen, I.D., Bromme, D., Cleutjens, K.B., Heeneman, S., Peters, C., Reinheckel, T., Saftig, P., Beertsen, W., 2006. Osteoclastic bone degradation and the role of different cysteine proteinases and matrix metalloproteinases: differences between calvaria and long bone. J. Bone Miner. Res. 21, 1399–1408.
Fedorowicz, Z., van Zuuren, E.J., Schoones, J., 2013. Botulinum toxin for masseter hypertrophy. Cochrane Database Syst. Rev. C, D007510.
Herring, S.W., 2003. TMJ anatomy and animal models. J. Musculoskelet. Neuronal. Interact. 3, 391–394, discussion 406–397.
Kun-Darbois, J.D., Libouban, H., Chappard, D., 2015. Botulinum toxin in masticatory muscles of the adult rat induces bone loss at the condyle and alveolar regions of the mandible associated with a bone proliferation at a muscle enthesis. Bone 77, 75–82.
Lodberg, A., Vegger, J.B., Jensen, M.V., Larsen, C.M., Thomsen, J.S., Bruel, A., 2015. Immobilization induced osteopenia is strain specific in mice. Bone Rep. 2, 59–67.
Mack, S.A., Maltby, K.M., Hilton, M.J., 2014. Demineralized murine skeletal histology. Methods Mol. Biol. 1130, 165–183.
Macpherson, P.C., Wang, X., Goldman, D., 2011. Myogenin regulates denervation-dependent muscle atrophy in mouse soleus muscle. J. Cell. Biochem. 112, 2149–2159.
Marchand-Libouban, H., Le Drevo, M.A., Chappard, D., 2013. Disuse induced by botulinum toxin affects the bone marrow expression profile of bone genes leading to a rapid bone loss. J. Musculoskelet. Neuronal. Interact. 13, 27–36.
Marino, S., Staines, K.A., Brown, G., Howard-Jones, R.A., Adamczyk, M., 2016. Models of ex vivo explant cultures: applications in bone research. Bonekey Rep. 5, 818.
Meng, H., Janssen, P.M., Grange, R.W., Yang, L., Beggs, A.H., Swanson, L.C., Cossette, S.A., Frase, A., Childers, M.K., Granzier, H., Gussoni, E., Lawlor, M.W., 2014. Tissue triage and freezing for models of skeletal muscle disease. J. Vis. Exp. 89, e51586.
Michailovici, I., Eigler, T., Tzahor, E., 2015. Craniofacial muscle development. Curr. Top. Dev. Biol. 115, 3–30.
Miller, J., Clarkson, E., 2016. Botulinum toxin type a: review and its role in the dental office. Dent. Clin. North Am. 60, 509–521.
Moon, Y.M., Kim, Y.J., Kim, M.K., Kim, S.G., Kweon, H., Kim, T.W., 2015. Early effect of Botox-A injection into the masseter muscle of rats: functional and histological evaluation. Maxillofac. Plast. Reconstr. Surg. 37, 46.
Murphy, K.T., Chee, A., Trieu, J., Naim, T., Lynch, G.S., 2012. Importance of functional and metabolic impairments in the characterization of the C-26 murine model of cancer cachexia. Dis. Model Mech. 5, 533–545.
Pfaffl, M.W., 2001. A new mathematical model for relative quantification in real-time RT-PCR. Nucleic Acids Res. 29, e45.
Pirazzini, M., Rossetto, O., Eleopra, R., Montecucco, C., 2017. Botulinum neurotoxins: biology, pharmacology, and toxicology. Pharmacol. Rev. 69, 200–235.
Rafferty, K.L., Liu, Z.J., Ye, W., Navarrete, A.L., Nguyen, T.T., Salamati, A., Herring, S.W., 2012. Botulinum toxin in masticatory muscles: short- and long-term effects on muscle, bone, and craniofacial function in adult rabbits. Bone 50, 651–662.
Raphael, K.G., Tadinada, A., Bradshaw, J.M., Janal, M.N., Sirois, D.A., Chan, K.C., Lurie, A.G., 2014. Osteopenic consequences of botulinum toxin injections in the masticatory muscles: a pilot study. J. Oral Rehabil. 41, 555–563.
Recidoro, A.M., Roof, A.C., Schmitt, M., Worton, L.E., Petrie, T., Strand, N., Ausk, B.J., Srinivasan, S., Moon, R.T., Gardiner, E.M., Kaminsky, W., Bain, S.D., Allan, C.H., Gross, T.S., Kwon, R.Y., 2014. Botulinum toxin induces muscle paralysis and inhibits bone regeneration in zebrafish. J. Bone Miner. Res. 29, 2346–2356.
Rossetto, O., Pirazzini, M., Montecucco, C., 2014. Botulinum neurotoxins: genetic, structural and mechanistic insights. Nat. Rev. Microbiol. 12, 535–549.
Sambasivan, R., Kuratani, S., Tajbakhsh, S., 2011. An eye on the head: the development and evolution of craniofacial muscles. Development 138, 2401–2415.
Santagati, F., Rijli, F.M., 2003. Cranial neural crest and the building of the vertebrate head. Nat. Rev. Neurosci. 4, 806–818.
Schiaffino, S., Reggiani, C., 2011. Fiber types in mammalian skeletal muscles. Physiol. Rev. 91, 1447–1531.
Schneider, C.A., Rasband, W.S., Eliceiri, K.W., 2012. NIH Image to ImageJ: 25 years of image analysis. Nat. Methods 9, 671–675.
Sciote, J.J., Horton, M.J., Rowlerson, A.M., Link, J., 2003. Specialized cranial muscles: how different are they from limb and abdominal muscles? Cells Tissues Organs 174, 73–86.
Sims, N.A., Martin, T.J., 2014. Coupling the activities of bone formation and resorption: a multitude of signals within the basic multicellular unit. Bonekey Rep. 3, 481.
Soares, A., Andriolo, R.B., Atallah, A.N., da Silva, E.M., 2014. Botulinum toxin for myofascial pain syndromes in adults. Cochrane Database Syst. Rev. C, D007533.
Spassov, A., Toro-Ibacache, V., Krautwald, M., Brinkmeier, H., Kupczik, K., 2017. Congenital muscle dystrophy and diet consistency affect mouse skull shape differently. J. Anat. 231 (5), 736–748.
Suzuki, A., Iwata, J., 2016. Mouse genetic models for temporomandibular joint development and disorders. Oral Dis. 22, 33–38.
Swanson, C., Lorentzon, M., Conaway, H.H., Lerner, U.H., 2006. Glucocorticoid regulation of osteoclast differentiation and expression of receptor activator of nuclear factor-kappaB (NF-kappaB) ligand, osteoprotegerin, and receptor activator of NF-kappaB in mouse calvarial bones. Endocrinology 147, 3613–3622.

Takahashi, N., Udagawa, N., Suda, T., 1999. A new member of tumor necrosis factor ligand family, ODF/OPGL/TRANCE/RANKL, regulates osteoclast differentiation and function. Biochem. Biophys. Res. Commun. 256, 449–455.

Thabane, L., Ma, J., Chu, R., Cheng, J., Ismaila, A., Rios, L.P., Robson, R., Thabane, M., Giangregorio, L., Goldsmith, C.H., 2010. A tutorial on pilot studies: the what, why and how. BMC Med. Res. Methodol. 10, 1.

Tinastepe, N., Kucuk, B.B., Oral, K., 2015. Botulinum toxin for the treatment of bruxism. Cranio 33, 291–298.

Tiphaine, C., Yaowalak, C., Cyril, C., Helder, G.R., Jacques, M., Paul, T., Monique, V.L., Laurent, V., Vincent, L., 2013. Correlated changes in occlusal pattern and diet in stem Murinae during the onset of the radiation of Old World rats and mice. Evolution 67, 3323–3338.

Toro-Ibacache, V., O'Higgins, P., 2016. The effect of varying jaw-elevator muscle forces on a finite element model of a human cranium. Anat. Rec. (Hoboken) 299, 828–839.

Valladares, D., Almarza, G., Contreras, A., Pavez, M., Buvinic, S., Jaimovich, E., Casas, M., 2013. Electrical stimuli are anti-apoptotic in skeletal muscle via extracellular ATP: alteration of this signal in Mdx mice is a likely cause of dystrophy. PLoS One 8, e75340.

van 't Hof, R.J., Rose, L., Bassonga, E., Daroszewska, A., 2017. Open source software for semi-automated histomorphometry of bone resorption and formation parameters. Bone 99, 69–79.

Vegger, J.B., Bruel, A., Dahlgaard, A.F., Thomsen, J.S., 2016. Alterations in gene expression precede sarcopenia and osteopenia in botulinum toxin immobilized mice. J. Musculoskelet. Neuronal. Interact. 16, 355–368.

Warner, S.E., Sanford, D.A., Becker, B.A., Bain, S.D., Srinivasan, S., Gross, T.S., 2006. Botox induced muscle paralysis rapidly degrades bone. Bone 38, 257–264.